Noname manuscript No.
(will be inserted by the editor)

Advanced modeling and simulation of SMC processes

M. Perez, D. Prono, C. Ghnatios, E. Abisset, J.L. Duval, F. Chinesta

Received: date / Accepted: date

Abstract In SMC processes, a charge of a composite material, which typically consists of a matrix composed of an unsaturated polyester or vinylester, reinforced with chopped glass fibres or carbon fibre bundles and fillers, is placed on the bottom half of the preheated mould. The charge usually covers 30 to 90% of the total area. The upper half of the mould is closed rapidly at a speed of about 40 mm/s. This rapid movement causes the charge to flow inside the cavity. The reinforcing fibres are carried by the resin and experience a change of configuration during the flow. This strongly influences the mechanical properties of the final part. Several issues compromises its efficient numerical simulation, among them: (i) the modeling of flow kinematics able to induce eventual fibres/resin segregation, (ii) the confined fibres orientation evolution and its accurate prediction, (iii) local dilution effects, (iv) flow bifurcation at junctions and its impact on the fibres orientation state, (v) charge / mould contact and (vi) parametric solutions involving non-interpolative fields. The present paper reports advanced modeling and simulation techniques for circumventing, or at least alleviating, the just referred difficulties.
Keywords: SMC, Confined orientation, Friction, Parametric solutions, PGD.

M. Perez, D. Prono & J.L. Duval @ ESI Group, 3bis rue Saarinen, 94528 Rungis cedex, France
E-mail: Marta.PerezMiguel@esi-group.com
E-mail: David.Prono@esi-group.com
E-mail: Jean-Louis.Duval@esi-group.com
C. Ghnatios @ Norte Dame University-Louaize, Mechanical engineering department, Zouk Mosbeh, Lebanon
E-mail: cghnatios@ndu.edu.lb
E. Abisset @ I2M, ENSAM ParisTech, Esplanade des Arts et Mtiers, 33405 Talence Cedex
E-mail: emmanuelle.abisset@ensam.eu
F. Chinesta @ ESI Group chair, PIMM Lab, ENSAM ParisTech, 151 Boulevard de l'Hôpital, 75013 Paris, France
E-mail: Francisco.Chinesta@ensam.eu
Corresponding author: Francisco Chinesta, Francisco.Chinesta@ensam.eu

1 Introduction

Over the last decades, an increasing number of functional and structural parts, made so far with metals, has been progressively reengineered by replacing metallic materials by polymers, reinforced polymers and composites. The motivation for this substitution may be the weight reduction, the simpler, cheaper or faster forming process, or the ability to exploit additional functionalities. The fillers usually employed cover a broad range involving many scales: (i) the nanometer scale (e.g. carbon nanotubes, graphene, fullerene, nanodiamonds); (ii) the micrometer to the millimeter scale (particles and short fibres); (iii) the centimeter scale of fibres used in SMC and BMC composite processes; and finally (iv) the macroscopic scale where fibrous reinforcements are made of continuous fibres arranged in bundles. When load-bearing capacities are especially looked for, continuous fibre reinforced polymers are selected. In that case, the impregnation of the reinforcement with a low viscosity polymer involves the flow of a Newtonian or non-Newtonian fluid in the complex multi-scale microstructure related to the fibre and tow arrangement.

Reinforced polymers are selected instead of high-performance polymers of equivalent properties since the latter are generally more expensive. When looking for functional properties, the use of nano-charges opens a wide spectrum of possibilities but also raises new challenges, such as dispersion of charges into the polymer matrix and occurrence of aggregation and disaggregation mechanisms. Suspensions of practical interest involve many scales and many concentration regimes, the latter ranging from dilute to highly concentrated.

This paper focusses on discontinuous fibre reinforcements and all along it the word "concentration" will refer to the density of fibre interactions. The flow regime here addressed consists of a squeeze flow induced by the suspension compression. Even if the flow of a suspension does not affect "a priori" the volume fraction of fibres (except in regions in which segregation mechanisms appear), when the squeeze progresses the density of fibre interaction along the gap thickness (that continuously decreases due to the compression) increases considerably, and at the end many solid bridges across the gap thickness appear preventing the compression from progressing.

This kind of flow regimes is the one encountered in composites processing like compression moulding or SMC largely considered in the automotive industry because of its high volume capabilities. In SMC processes, a charge of a composite material, which typically consists of a matrix composed of an unsaturated polyester or vinylester, reinforced with chopped glass fibres or carbon fibre bundles and fillers, is placed on the bottom half of the preheated mould. The charge usually covers 30 to 90% of the total area. The upper half of the mould is closed rapidly at a speed of about 40 mm/s. This rapid movement causes the charge to flow inside the cavity. The reinforcing fibres are carried by the resin and experience a change of configuration during the flow. This strongly influences the mechanical properties of the final part.

The process simulation must track the entire fluid flow history in order to be able to predict the final reinforcement structure, and subsequently, the in-

duced mechanical properties. Compression moulding of SMC can also generate several defects. Among them, (i) inappropriate fibre orientation with respect to the optimal one; (ii) segregation that results in regions in which the resin appears devoid of fibres; (iii) global filling defects originated by inappropriate placement, shape and orientation of the charge into the mould, etc.

After this short introduction Section 2 focuses on the confined orientation modeling, that will integrated in Section 3 with an unified flow model covering the different flow regimes. Then Section 4 addresses fibre dilution, Section 5 charge / mould interaction and Section 6 addressed the modeling of diverging flows at part junctions. Finally Section 7 proposes a parametric approach. Different illustrators are included in each section. The natural continuation of the present paper, devoted to model calibration and validation constitutes a work in progress.

2 Modeling flow induced confined orientation

In this section we revisit the modeling of the flow induced orientation at different scales (micro, meso and macro), different descriptions (discrete and continuous) and different regimes (dilute and concentrated) while considering confinement effects.

2.1 Microscopic description of confined kinematics of an individual fibre

It is well known that the kinematics of a fibre with infinite aspect ratio (assimilated to a rod), immersed in an unconfined flow characterized by the velocity gradient $\nabla\mathbf{v}$, is given by Jeffery's equation [20]

$$\dot{\mathbf{p}} = \nabla\mathbf{v}\cdot\mathbf{p} - (\nabla\mathbf{v} : (\mathbf{p}\otimes\mathbf{p}))\mathbf{p}, \tag{1}$$

where $\mathbf{p}$ is the unit vector aligned with the rod axis.

When the domain thickness $2H$ is smaller than the rod length $2L$, i.e. $H < L$, some Jeffery's trajectories are forbidden, i.e. those trajectories involving $L\mathbf{p}\cdot\mathbf{n} > H$, where $\mathbf{n} = (0,0,1)^T$ is the unit vector defining the thickness direction. In that case, the rod kinematics is defined by the standard Jeffery model (1) while $\mathbf{p}\cdot\mathbf{n} < H/L$ and are perturbed as soon as the rod reaches the upper and lower walls. In order to determine the perturbed rod kinematics, we represent the rod as a dumbbell [1] with hydrodynamic and contact forces acting on the dumbbell beads, the last acting in the direction perpendicular to the wall (we thus ignore possible friction at the wall). Thus, by enforcing forces and torques balances, it finally results the extended Jeffery equation given the fibre rotary velocity $\dot{\mathbf{p}}$ [24]

$$\dot{\mathbf{p}} = \dot{\mathbf{p}}^J - \frac{1}{1-p_z^2}\left[\dot{\mathbf{p}}^J\right]_z (\mathbf{n} - p_z\ \mathbf{p}), \tag{2}$$

where $p_z = \mathbf{p}\cdot\mathbf{n}$ and $\dot{\mathbf{p}}^J$ denotes the Jeffery rotary velocity given by Eq. (1).

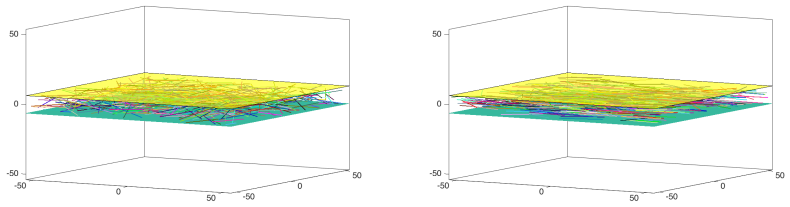

Fig. 1 DNS – Direct Numerical Simulation – of confined concentrated suspensions: (left) initial almost uniform confined orientation distribution and (right) almost steady state solution related to the unidirectional squeeze flow.

In [29] authors considered confined fibre kinematics in Poiseuille flows (close to those encountered in squeeze flows) by considering a second-gradient modeling framework.

2.2 Mesoscopic description of a population of rods

Having described the kinematics of individual rods in confined flows, we now turn to a population of non-interacting rods. There are two natural approaches for doing so, i.e. discrete and continuous:

1. The discrete approach consists in computing the orientation of each individual rod belonging to a large discrete ensemble of $\mathtt{N}$ rods. Thus, the population is described from the individuals composing it, whose conformation is given by vectors $\mathbf{p}_i, i = 1, ..., \mathtt{N}$, each governed by Eq. (2). The main drawback of this approach lies in the necessity of tracking the evolution of each rod by solving the corresponding equation, and even if conceptually there is no major difficulty, the computing cost could be excessive in most practical applications.
   The computational complexity becomes even more stringent when considering concentrated regimes that require accounting for the numerous fibre interactions [6, 22, 23]. Some snapshots of such direct numerical simulations when considering confinement and fibres interactions in a representative flow cell are depicted in Fig. 1
2. The continuous approach when ignoring fibres interactions uses the pdf $\psi(\mathbf{x}, t, \mathbf{p})$ that gives the fraction of rods oriented along direction $\mathbf{p}$ at position $\mathbf{x}$ and time t. This description avoids the complexity related to the immense number of fibres involved in suspensions of practical interest. The pdf satisfies the normalisation condition
   $$\int_{\mathcal{S}} \psi(\mathbf{x}, t, \mathbf{p})\ d\mathbf{p} = 1, \quad \forall \mathbf{x}, \quad \forall t, \tag{3}$$
   where $\mathcal{S}$ is the rod conformation space, i.e. the surface of the unit sphere. Conservation of probability leads to the so-called Fokker-Planck equation
   $$\frac{\partial \psi}{\partial t} + \nabla_x \cdot (\dot{\mathbf{x}}\ \psi) + \nabla_p \cdot (\dot{\mathbf{p}}\ \psi) = 0, \tag{4}$$

where the rod rotary velocity $\dot{\mathbf{p}}$ is given by the confined Jeffery's equation (2) and $\dot{\mathbf{x}} = \mathbf{v}(\mathbf{x}, t)$.

2.3 Macroscopic description of a population of rods

Macroscopic models describe the suspension microstructure via suitable moments of the pdf, defined in standard physical domains involving space and time. These moments can be computed either via a discrete or continuous approach.

1. The discrete approach computes the pdf moments from adequate ensemble averages. For example the second order orientation tensor results [2]

$$\mathbf{a}^{disc}(t) = \frac{1}{\mathtt{N}} \sum_{i=1}^{\mathtt{N}} \mathbf{p}_i(t) \otimes \mathbf{p}_i(t), \tag{5}$$

   where the superscript *disc* refers to the discrete approach.
   The main disadvantage of this approach is the computational cost due to the extremely large number of particles to be considered.
2. In the continuous approach the pdf moments are evaluated analytically, from its continuous definition. In particular the second and fourth order orientation tensors (odd moments vanish in view of the symmetry of the pdf), $\mathbf{a}$ and $\mathbf{A}$ respectively, read:

$$\mathbf{a} = \int_{\mathcal{S}} \mathbf{p} \otimes \mathbf{p} \; \psi(\mathbf{x}, t, \mathbf{p}) \; d\mathbf{p}, \tag{6}$$

   and

$$\mathbf{A} = \int_{\mathcal{S}} \mathbf{p} \otimes \mathbf{p} \otimes \mathbf{p} \otimes \mathbf{p} \; \psi(\mathbf{x}, t, \mathbf{p}) \; d\mathbf{p}. \tag{7}$$

In practice continuous macroscopic descriptions are preferred in view of their computational simplicity. When ignoring confinement effects, the procedure described in [7] leads to

$$\dot{\mathbf{a}} = \nabla \mathbf{v} \cdot \mathbf{a} + \mathbf{a} \cdot (\nabla \mathbf{v})^T - 2 \; \mathbf{A} : \nabla \mathbf{v}. \tag{8}$$

In order to account for the intense randomizing effects induced by rods interaction, a diffusion term was added to the Fokker-Planck equation (4) [19] that results in an extra-term in the previous equation (8), leading to the so-called Folgar & Tucker model that in the case of a planar orientation reads [2]

$$\dot{\mathbf{a}} = \nabla \mathbf{v} \cdot \mathbf{a} + \mathbf{a} \cdot (\nabla \mathbf{v})^T - 2 \; \mathbf{A} : \nabla \mathbf{v} - 4 D_r \left(\mathbf{a} - \frac{\mathbf{I}}{2} \right). \tag{9}$$

When ignoring Brownian effects, the diffusion coefficient is assumed scaling with the second invariant of the strain rate tensor. To close the problem a closure relation expressing the fourth order orientation tensor as a fonction of the lower order ones (the second order here) is needed. The simplest ones

consist of the linear, quadratic and hybrid closure relations [3], even if more sophisticated choices exist as reported in our former work [7] and discussed in [23] in the context of confined flows.

Considering confinement at the macroscopic scale involves many difficulties related to the appearance of other tensors whose time evolution induce closure issues never until now addressed [24]. In [23] a deep analysis was performed from which it was concluded that the main deviations between discrete simulations (assumed as reference) and the one obtained by using the different macroscopic models was mainly due to the inability of representing confined orientations by using low order orientation tensors. This inability could also be at the origin of the orientation delay experimentally noticed and that was at the origin of different enrichment of orientation kinetics and the diffusion term reported in [32,33,26]. Thus, it was concluded that the most valuable macroscopic modeling route consists of using the state-of-the-art models (e.g. Flogar & Tucker) and constructing empirical closure relations by enforcing the agreement between the macroscopic predictions performed by using both discrete and continuous models. Empirical closures were considered in the derivation of the natural and the IBOF, among other fitted closures [17,13,21,27,18].

Considering the part depicted in Fig. 2, four charges were initially placed in the four corners and squeezed with a constant velocity of 2 mm/s. Each charge had a volume of (850 x 11) mm^3 and fiber orientation was assumed initially isotropic. Resin viscosity was considered 0.1 Pa·s. Fig. 2 depicts the final snapshot of the orientation field related to squeezed charges considering the planar component of the standard Folgar & Tucker model [19] complemented with a quadratic closure relation. The results shown in Fig. 2 correspond to $\lambda_{max}\mathbf{t}$, being $\mathbf{t}$ the eigenvector associated to the highest eigenvalue λ_{max} of the planar orientation tensor value $\mathbf{a}$ at each element.

3 Flow modeling

When analyzing the process experimentally, three different flow regimes are identified. It is expected that at very low density of inter-fibre contacts, and as predicted by standard suspension models, fibres move with the suspending fluid velocity. When the density of fibre interactions becomes extremely high and a percolated network of fibre contacts is established within the suspension, fibres cannot move anymore and then the fluid flows throughout the rigid or moderately deformable entangled fibres skeleton, like a fluid flowing through a porous medium. In between these two limit cases, one could expect that fibres move but with a velocity lower than the one of the suspending fluid, and therefore two contributions are expected, one coming from standard suspension theory in which fibres and fluid move with the same velocity, and the other resulting in a Darcy contribution consisting of the relative fibres/fluid velocity.

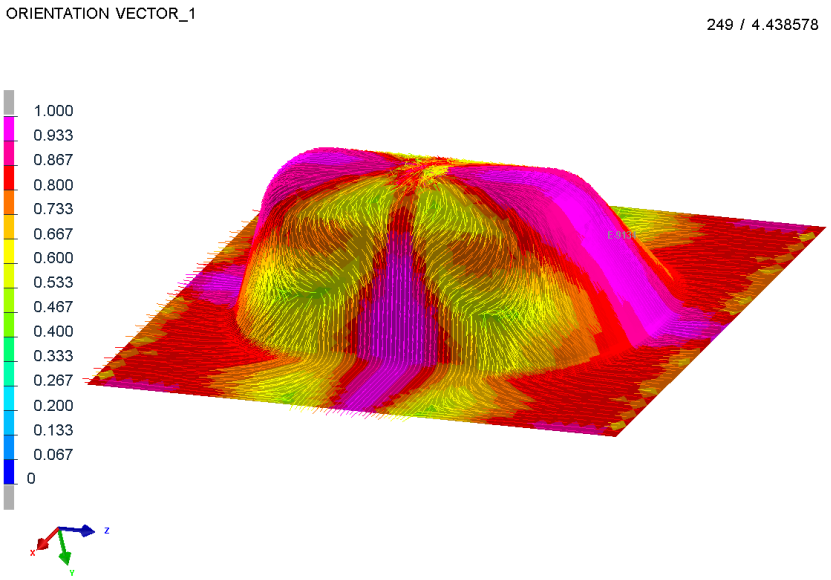

Fig. 2 Orientation field computed with the planar component of the Folgar & Tucker model for a composite part. Color refers to the value of the highest eigenvalue, and consequently can be interpreted as the intensity of the orientation along the direction indicated by the depicted vectors.

3.1 Generalized model bridging all flow regimes

As just indicated when approaching the percolated regime, where intense hydrodynamic interactions and contacts occur, the relative velocity between the fibres and the suspending fluid results in fluid / fiber segregation.

In this flow regime we can assume that the flow consists of one contribution coming from the flowing suspension with a velocity that coincides with the one of the fibres, and another in which the fibres are assumed at rest and the fluid flows through the fibrous skeleton with the fluid/fibres relative velocity. The fluid velocity is denoted by $\mathbf{v}$, the one of the fibres that defines the suspension velocity by $\mathbf{v}^s$, and the relative velocity of the fluid with respect to the fibres by $\mathbf{v}^d$ (the Darcy contribution). As discussed in [25] we have the equalities:

$$\begin{cases} \mathbf{v} = \mathbf{v}^s + \mathbf{v}^d \\ \mathbf{v}^s = \alpha \mathbf{v} \\ \mathbf{v}^d = (1-\alpha)\mathbf{v} \end{cases}, \tag{10}$$

where $\alpha \approx 1$ in the dilute regime whereas it almost vanishes when a dense contact network occurs.

Now, we consider the pressure drop related to both flow contributions, the one of the suspension flowing at velocity $\mathbf{v}^s$,

$$\nabla P^s = \eta \Delta \mathbf{v}^s + 2\eta N_p \nabla \cdot ((\mathbf{D}^s : \mathbf{a})\mathbf{a}) \,, \tag{11}$$

where the first term of the r.h.s. account for the viscous effects whereas the last one represents the extra-stresses due to the fibres presence and orientation. In this expression η represents the resin viscosity, $\mathbf{D}^s$ the rate of stain tensor related to the suspension velocity field $\mathbf{v}^s$ and N_p depends on the fibre concentration and fibre aspect ratio.

Then, the one related to the Darcy contribution reads

$$\nabla P^d = -\mathbf{K}^{-1}(\mathbf{a}) \cdot \mathbf{v}^d, \tag{12}$$

where $\mathbf{K}$ represents the permeability that at its turn depends on the fibre arrangement (fibres concentration and orientation).

Adding both pressure drops for obtaining the total one,

$$\nabla P = \nabla P^s + \nabla P^d = \eta \Delta \mathbf{v}^s + 2\eta N_p \nabla \cdot ((\mathbf{D}^s : \mathbf{a})\mathbf{a}) - \mathbf{K}^{-1}(\mathbf{a}) \cdot \mathbf{v}^d, \tag{13}$$

and writing both velocities $\mathbf{v}^s$ and $\mathbf{v}^d$ as a function of the total fluid velocity $\mathbf{v}$ according to Eq. (10), it finally results

$$\nabla P = \alpha \left\{ \eta \Delta \mathbf{v} + 2\eta N_p \nabla \cdot ((\mathbf{D} : \mathbf{a})\mathbf{a}) \right\} - (1-\alpha) \left\{ \mathbf{K}^{-1}(\mathbf{a}) \cdot \mathbf{v} \right\}. \tag{14}$$

This has the form of the Brinkmann model where the viscous and Darcy contributions are weighted by the factors α and $(1-\alpha)$ respectively, with α depending, as previously indicated, on the density of fibre interactions. Parameter α plays a crucial role, and it must be addressed by using finer micromechanical analyses [15,16,28,30,31,34] and the associated experimental calibration.

3.2 Lubrication approximation

In the case of narrow gaps, lubrication theory implies a computationally valuable dimensionality reduction. First, we consider the viscous contribution, where for the sake of simplicity we ignore the anisotropic term, i.e. we assume $N_p = 0$ (even if it could be easily retained). Thus, we have

$$\nabla P^s = \eta \Delta \mathbf{v}^s. \tag{15}$$

Lubrication approximation states that the velocity gradients in the thickness direction are much larger than in-plane gradients, and that the through-the-thickness velocity component can be neglected with respect to the in-plane components. Following [25], pressure becomes independent on the thickness coordinate, i.e. $P = P(x, y)$ and by enforcing no-slip boundary conditions at both gap walls the velocity field reads

$$\mathbf{v}^s(x, y, z) = \frac{1}{2\eta} \nabla P^s (z^2 - H^2), \tag{16}$$

where the gap thickness is $2H$.

By averaging velocity across the gap thickness it results

$$\tilde{\mathbf{v}}^s(x, y) = \frac{1}{2H} \int_{-H}^{+H} \mathbf{v}(x, y)\, dz = -\frac{H^2}{3\eta} \nabla P^s, \tag{17}$$

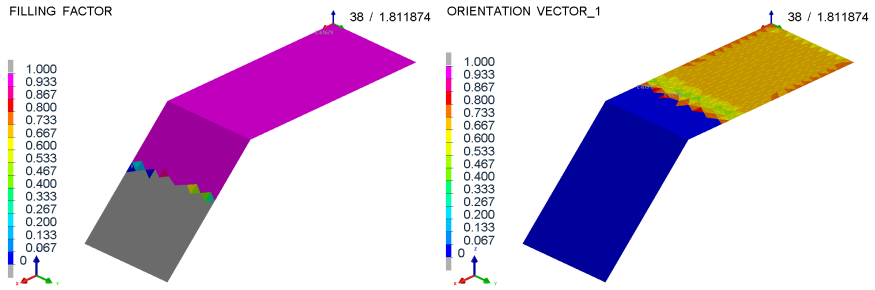

Fig. 3 Induced segregation: (left) resin front position and (right) charge (resin and fibres mixture) position.

the previous equation can be rewritten as

$$\nabla P^s = -\frac{3\eta}{H^2}\tilde{\mathbf{v}}^s, \tag{18}$$

that with the Darcy contrubution

$$\nabla P^d = -\mathbf{K}^{-1}(\mathbf{a}) \cdot \tilde{\mathbf{v}}^d, \tag{19}$$

leads to

$$\nabla P = -\frac{3\eta}{H^2}\tilde{\mathbf{v}}^s - \mathbf{K}^{-1}(\mathbf{a}) \cdot \tilde{\mathbf{v}}^d, \tag{20}$$

or

$$\nabla P = -\alpha\frac{3\eta}{H^2}\tilde{\mathbf{v}} - (1-\alpha)\mathbf{K}^{-1}(\mathbf{a}) \cdot \tilde{\mathbf{v}}. \tag{21}$$

The flow model must be complemented with the one governing the evolution of the fluid phase field needed for defining the flow domain at each time $\Omega_f(t)$ [25] (a deep discussion on the flow domain updating was performed in [7]),

$$\frac{DI}{Dt} = 0. \tag{22}$$

To numerically check the just derived model, the position of both the resin and charge (resin and fibres mixture) fronts was simulated while squeezing the charged resin with a constant compression velocity of 10 mm/s. The volume of the reinforced resin was (300 x 300 x 30) mm^3 and resin viscosity was considered 0.1 Pa·s. The inital fiber orientation was considered isotropic. By choosing intermediate values of the alpha parameter, i.e. $0 < \alpha < 1$, segregation was induced as noticed in Fig. 3. In this simulation the orientation evolution was assumed governed by the standard Folgar & Tucker model addressed in the previous section.

4 Modeling dilution effects

It has been observed that SMC processes can induce segregation, previously addressed, in some cases accompanied by a certain fibre dilution at the flow front neighborhood. The model proposed for explaining segregation considers that the suspension has a uniform fibre concentration. In what follows we propose a model that describe the fibre concentration evolution that allows explaining fibre dilution.

We assume that the generalized Brinkmann model, previously opresented, computes the pressure and velocity fields, P and $\mathbf{v}$ respectively. The suspension velocity results $\mathbf{v}^s = \alpha\mathbf{v}$. Moreover, we can assume that the density of inter-fibre contacts $\mathcal{C}$ scales with $1-\alpha$.

The contacts balance reads

$$\frac{\partial \mathcal{C}}{\partial t} + \mathbf{v}^s \cdot \nabla \mathcal{C} = \mathtt{c}(\mathbf{a}, \phi, \mathcal{U}), \tag{23}$$

where $\mathtt{c}(\mathbf{a}, \phi, \mathcal{U})$ is the density of contacts generated when squeezing the suspension with fibre concentration ϕ at compression rate $\mathcal{U}$, being the local orientation given by $\mathbf{a}(\mathbf{x})$.

This equation allows evaluating the evolution of the density of contacts everywhere in the domain, i.e. $\mathcal{C}(\mathbf{x}, t)$, and with it update the value of α, being $\mathcal{C} \propto (1-\alpha)$, as well as its spatial gradient $\nabla\alpha$.

Now, using $\mathbf{v}^s = \alpha\mathbf{v}$, the fibre balance writes

$$\frac{\partial \phi}{\partial t} + \alpha\mathbf{v} \cdot \nabla\phi + \phi\mathbf{v} \cdot \nabla\alpha = 0, \tag{24}$$

that allows updating the fibre concentration.

5 Modeling the interaction between the charge and the mould

Today the choice of the boundary condition to be enforced at the walls when simulating SMC processes remains quite controversial.

When considering the flow in narrow gaps, lubrication theory implies a computationally valuable dimensionality reduction. We assume (x, y) the in-plane coordinates whereas z denotes the out-of-plane one, associated to the thickness, with $\mathbf{x} = (x, y)^T \in \Omega \subset \mathbb{R}^2$ and $z \in \mathcal{I} = [-H, H]$, with $H \ll \mathcal{L}$ (being $\mathcal{L}$ the characteristic in-plane dimension, $|\Omega| = \mathcal{L}^2$).

If the flow is assumed viscous (segregation is neglected in this section) with an effective viscosity accounting for the presence of fibers, the flow model becomes described by the so-called Stokes equations

$$\nabla p = \eta \Delta \mathbf{v}, \tag{25}$$

with the velocity components $\mathbf{v} = (u, v, w)^T$ and where p denotes the pressure field.

The consideration of lubrication hypotheses in Eq. (25) results in

$$\begin{cases} \frac{\partial u}{\partial z} = \frac{1}{\eta}\frac{\partial p}{\partial x} z \\ \frac{\partial v}{\partial z} = \frac{1}{\eta}\frac{\partial p}{\partial y} z \end{cases} . \tag{26}$$

Now, by multiplying Eq. (26) by the viscosity and particularizing it at the wall $z = H$, the shear at the wall $\boldsymbol{\tau}_w$ is obtained

$$\boldsymbol{\tau}_w = H \nabla p. \tag{27}$$

In what follows the stress and velocity at the wall are noted by $\boldsymbol{\tau}_w$ and $\mathbf{v}_w$ respectively, both fulfilling the viscous friction law

$$\boldsymbol{\tau}_w = \mu \mathbf{v}_w. \tag{28}$$

Now, integrating Eq. (26) and taking into account that the velocity at the wall writes $\mathbf{v}_w$, it results

$$\mathbf{v} = \frac{1}{2\eta} \nabla p \left(z^2 - H^2\right) + \mathbf{v}_w. \tag{29}$$

By integrating the velocity along the thickness, it results the flow rate $\mathbf{Q}$, from which the mass balance reads

$$\nabla \cdot \mathbf{Q} = \mathcal{U}, \tag{30}$$

or more explicitly

$$\left(-\frac{2H^3}{3\eta} + \frac{2H^2}{\mu}\right) \Delta p = \mathcal{U}, \tag{31}$$

where $\mathcal{U}$ is the compression rate.

The implementation of the lubricated friction law is straightforward, requiring a minimum number of changes as the observation of Eq. (31) reveals. When considering the simplest viscous friction law (linear and isotropic), squeeze flow assuming stick contact conditions generates, as expected, higher pressures than when considering the viscous friction as Fig. 4 proves. Both results show a snapshot of the pressure field related to a squeezed charge, of initial square shape and volume of (300 x 300 x 5) mm^3. Resin viscosity was considered 0.1 Pa·s and the considered compression rate was 2.5 10^{-2} mm/s in both cases.

6 Modeling diverging flows at junctions

When addressing a T-junction nothing really changes in what concerns the flow model. The flow separation is addressed in the same manner that in the case of standard RTM process simulation because as proved before both mathematical models become almost the same as soon as we consider an effective permeability and a source term in the generalized Poisson problem when squeeze applies.

From the point of view of fibres orientation the situation is a bit more complex because one could easily visualize that only fibres aligned with the

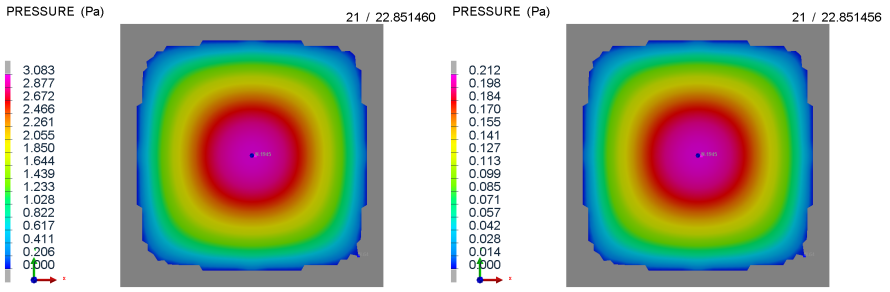

Fig. 4 Squeezing an initially squared charge when assuming sticking contact conditions (left) and viscous contact (right). A very different pressure map can be noticed by noting the different color scales.

rib can penetrate in it. The fact that only fibres adequately aligned with the rib enter in it means that the local state of orientation just after the T-junction differs to the one existing at its entrance.

To compute both downstream orientation states we proceed as follows:

- The orientation tensor at the upstream elements is diagonalized;
- The planar orientation tensor can be expressed in the principal directions from the rotation associated to the tensor eigenvectors;
- The principal axes are projected (with their lengths scaling with their corresponding eigenvalues) on the rib planar direction;
- The projections weighted by a scalar β, $0 < \beta < 1$, are removed from the diagonal tensor. The β coefficient expresses that not all the fibres aligned with the rib penetrate in it, some fibres, strongly entangled with others with different orientations, are prevented to do it;
- The new tensor related to the downstream element in the rib, and the one downstream in the plate are normalized to have unit traces;
- Then the one assigned to the downstream element on the plate is pushed-back to the initial frame (by applying the inverse rotation);
- Fibres concentration reduction (the complementary quantity being the one coming into the rib) can be evaluated from the projected principal orientations affected by the weight β.

A view of the resulting flow and orientation state in a T-junction, in agreement with the discussion just addressed, is depicted in Fig. 5. The charge, assumed initially isotropic, was squeezed with a constant velocity of 2 mm/s. The volume of the reinforced fluid was (1000 x 150 x 9) mm^3 and resin viscosity was considered 0.1 Pa·s.

7 Parametric solutions

In this final section we address the construction of parametric solutions of SMC processes. These parametric solutions could involve any of the model

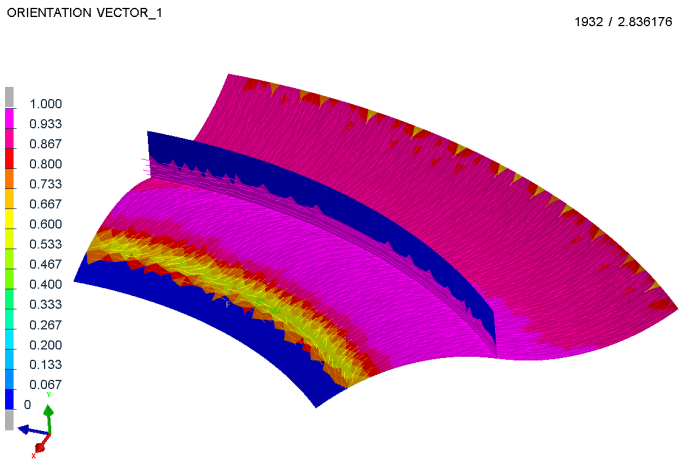

Fig. 5 T-junction and its corresponding flow bifurcation and fibres orientation updating.

parameters to create a sort of computational *vademecum* allowing the online evaluation of the model (under the stringent real-time constraints) for any possible choice of the parameters that were introduced in the parametric model and then in its associated parametric solution.

PGD-based Model Order Reduction allows computing offline, using all the needed computational resources and computing time, a parametric solution that contains the solution of all possible scenarios. This parametric solution can then be online particularized to any scenario using deployed computational facilities, including tablets or even smartphones. It allows then to perform efficient simulation, optimization, inverse analysis, uncertainty propagation and simulation-based control, all under real-time constraints. Such a solution has been demonstrated on many applications where the Proper Generalized Decomposition (PGD) method is used [4,5,9–12] .

When the unknown field is a function of space, time and a number of parameters $\mu_1, \ldots, \mu_{\mathtt{Q}}$, the subsequent separated representation could be written as

$$u(\boldsymbol{x}, t, \mu_1, \ldots, \mu_{\mathtt{Q}}) \approx \sum_{i=1}^{\mathtt{M}} X_i(\boldsymbol{x}) T_i(t) \prod_{j=1}^{\mathtt{Q}} M_i^j(\mu_j). \tag{32}$$

The use of a separated representation allows circumventing the combinatorial explosion. The solution of a sequence of low-dimensional problems allows calculating the parametric solution that can be viewed as a chart, abacus or vademecum—or, simply, as a high-dimensional response surface—, to be used online in a variety of applications.

However the construction of separated representation becomes very intrusive and then, in order to make possible the use of existing commercial simulation softwares, we proposed recently different non-intrusive methodologies that from the solution of some offline calculations for given parameters,

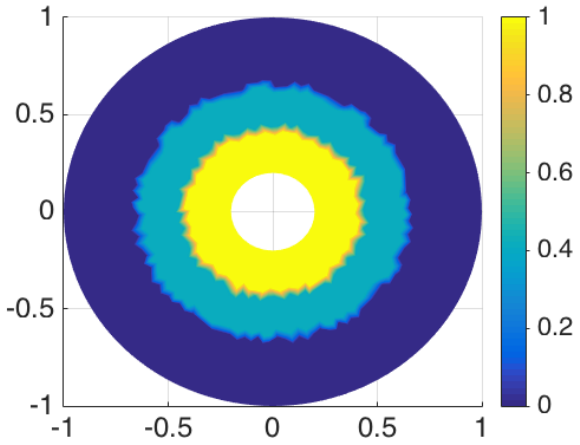

Fig. 6 Interpolated fluid domain from two solutions corresponding to two different squeezing rates.

allows interpolating for any other choice of parameters. In our former works we widely considered the so-called SSL-PGD [8]. However, such a procedure fails when solution exhibits strong localization as discussed below.

7.1 Interpolation issues and interpolative mappings

Imagine for a while that the solution of a parametric model localizes around $\mathbf{X}_1$ when using a value μ_1 of the model parameter. Then, when considering parameter μ_2 the solution localizes around $\mathbf{X}_2$. Thus, one can expect, based on a physical sense, that when considering $\mu_3 = 0.5\mu_1 + 0.5\mu_2$, the solution should localize around $\mathbf{X_3}$, the middle point on the segment joining $\mathbf{X}_1$ and $\mathbf{X}_2$. However, standard interpolation, as the one considered by non-intrusive parametric solution constructors, fails, and instead of giving that expected solution, it produced one composed of a half of the first (localizing around $\mathbf{X}_1$) and a half of the second one localizing around $\mathbf{X}_2$.

This is exactly what happens when considering for example the squeeze of a circular charge (fibre/resin mixture) with two different compression rates. The higher is the compression rate, the higher the radius of the squeezed charge at a given time. If now, from the solution for two different values of the compression rate, i.e. the respective radius of the squeezed charges at a given time, we want to infer the one related to an intermediate compression rate and we proceed by a simple standard interpolation of both solutions, the interpolated solution exhibits two spurious flow fronts, the ones related to each solution that were combined by the interpolation. Figure 6 depicts such an unphysical situation. To circumvent that issue we propose the use of the so-called interpolative mapping described below.

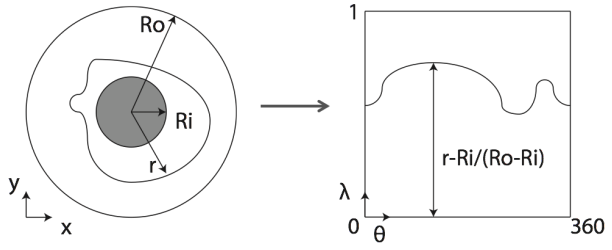

Fig. 7 Flow fronts interpolative mapping

7.2 Flow front mapping

To address the interpolation of fields defined in different domains, the idea is to map them into a unique reference domain, where interpolation could be safely performed, and then push-back the interpolated solution.

To describe that mapping we consider the scenario depicted in Fig. 7. Knowing the internal and external radius (for example the ones associated to two different compression rates), R_i and R_o respectively, we can define the domain in between by considering the coordinates (λ, θ), with $\theta \in [0, 2\pi]$ and $\lambda \in [0, 1]$, and any front in between described from

$$\lambda(\theta) = \frac{r(\theta) - R_i}{R_o - R_i}, \tag{33}$$

where the internal and external fronts are related to the $\lambda = 0$ and $\lambda = 1$ values respectively. In the most general case we will have $R_i(\theta)$ and $R_o(\theta)$.

Now, if the external front R_o was associated to a compression rate $\mathcal{U}_o$ and the internal one to $\mathcal{U}_i$ a more physical solution of an intermediate value, for example $\mathcal{U} = 0.5\mathcal{U}_o + 0.5\mathcal{U}_i$, will be a front located in the middle, i.e. $\lambda = 0.5$. The same process can be performed by constructing the level-set related to those flow fronts and then interpolating them.

When the solution has not a linear dependence on the parameter, linear interpolation could fail, but the accuracy could be improved using nonlinear interpolations or by enriching the sampling, but in all cases interpolation artefacts are avoided, as Fig. 8 proves when compared with Fig. 6.

7.3 Charge location as parameter

In this case we address the situation in which the location of the charge differs. Thus, knowing for instance four solutions, related to the compression of the charge placed at four different locations, we would like infering the compression of the charge now located at any other position in the mould.

For that purpose the interpolative mapping proceeds by defining a reference location (see Fig. 9) and mapping the four known solutions to it. Then, interpolation is performed and the solution pushed-back to any location. The

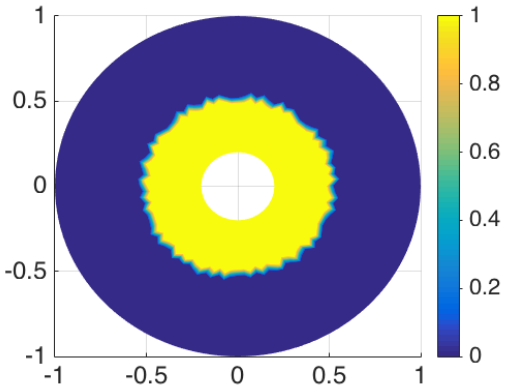

Fig. 8 Predicted flow front by using the interpolative mapping

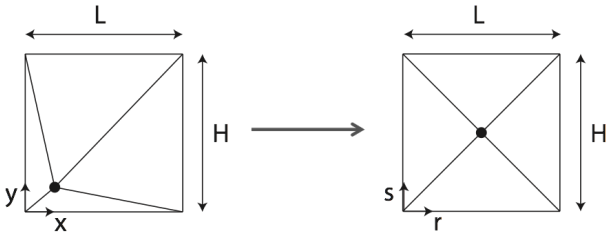

Fig. 9 Interpolative mapping for solutions associated to different charge locations.

mapping is illustrated in Fig. 9 where the known solutions in the (x, y) coordinate system are mapped to the coordinate system (r, s) in which the charge is always placed at its centre. In the present case the mapping is extremely simple because it consists of a linear transformation of each of the four considered triangles, all them having a constant Jacobian. Solutions associated with standard interpolation as well as to the use of interpolative mapping just described are depicted in Fig. 10, where it can be noticed that the last procedure allows avoiding numerical artefacts.

8 Conclusions

This paper presented an advanced numerical modeling of SMC processes by integrating different original functionalities, most of them never considered in the existing SMC numerical models. In particular the proposed solution concerns:

- A flow model that results into a Brinkmann equation based on fine scale micromechanical considerations;
- That model accepts a simple formulation within the lubrication regime that simply requires the use of an effective permeability;

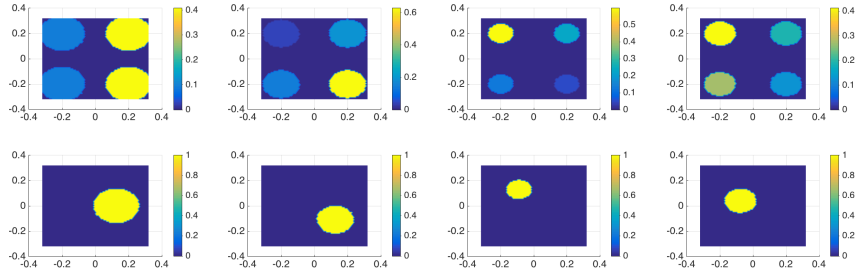

Fig. 10 Interpolating solutions related to flow domains associated to different locations of the squeezed charge: (top) standard interpolation exhibiting spurious solutions and (bottom) when performing the interpolative mapping.

- The flow model allows predicting segregation, with the use of a single micromechanical parameter that depends on the fibre interactions;
- The orientation model addresses confinement issues by employing a fitted closure relation in the Folgar & Tucker description;
- The issue of dilution has been addressed and linked to the gradient of the density of fibre contacts;
- The proposed model allows integrate in the formulation, without major difficulties, a lubricated friction at the charge / mould walls contact;
- The proposed approach has been adapted for addressing flow junctions, with special care on the fibre concentration and orientation updates;
- Finally the model has been extended for addressing parametric studies by defining an interpolative mapping to avoid numerical artefacts that standard interpolations produce.

Compliance with Ethical Standards. The authors declare that they have no conflict of interest.

References

1. E. Abisset-Chavanne, F. Chinesta, J. Ferec, G. Ausias, R. Keunings. On the multiscale description of dilute suspensions of non-Brownian rigid clusters composed of rods. Journal of Non-Newtonian Fluid Mech., **222**, 34-44 (2015).
2. S. Advani, Ch. Tucker. The use of tensors to describe and predict fibre orientation in short fibre composites. J. Rheol., **31**, 751-784, 1987.
3. S. Advani, Ch. Tucker. Closure approximations for three-dimensional structure tensors. J. Rheol., **34**, 367-386, 1990.
4. A. Ammar, B. Mokdad, F. Chinesta, R. Keunings. A new family of solvers for some classes of multidimensional partial differential equations encountered in kinetic theory modelling of complex fluids. J. Non-Newtonian Fluid Mech., **139**, 153-176, 2006.

5. A. Ammar, B. Mokdad, F. Chinesta, R. Keunings. A new family of solvers for some classes of multidimensional partial differential equations encountered in kinetic theory modelling of complex fluids. Part II: transient simulation using space-time separated representations. J. Non-Newtonian Fluid Mech., **144**, 98-121, 2007.
6. G. Ausias, X.J. Fan, R. Tanner. Direct simulation for concentrated fibre suspensions in transient and steady state shear flows. Journal of Non-Newtonian Fluid Mech., **135**, 46-57, 2006.
7. C. Binetruy, F. Chinesta, R. Keunings. Flows in polymers, reinforced polymers and composites. A multiscale approach. Springerbriefs, Springer, 2015.
8. D. Borzacchiello, J.V. Aguado, F. Chinesta. Non-intrusive sparse subspace learning for parametrized problems. Archives of Computational Methods in Engineering, In press.
9. F. Chinesta, A. Ammar, A. Leygue, R. Keunings. An overview of the Proper Generalized Decomposition with applications in computational rheology. Journal of Non Newtonian Fluid Mech., **166**, 578-592, 2011.
10. F. Chinesta, P. Ladeveze, E. Cueto. A short review in model order reduction based on Proper Generalized Decomposition. Archives of Computational Methods in Engineering, **18**, 395-404, 2011.
11. F. Chinesta, A. Leygue, F. Bordeu, J.V. Aguado, E. Cueto, D. Gonzalez, I. Alfaro, A. Ammar, A. Huerta. Parametric PGD based computational vademecum for efficient design, optimization and control. Archives of Computational Methods in Engineering, **20/1**, 31-59, 2013.
12. F. Chinesta, R. Keunings, A. Leygue. The Proper Generalized Decomposition for advanced numerical simulations. A primer. Springerbriefs, Springer, 2014.
13. D.H. Chung, T.H. Won. Improved model of orthotropic closure approximation for flow induced fiber orientation. Polymer Composites, **22/5**, 636-649 (2001).
14. J.S. Cintra, Ch.L. Tucker III. Orthotropic closure approximations for flow-induced fiber orientation. J. Rheol., **39/6**, 1095-1121 (1995).
15. M. Doi, S.F. Edwards. Dynamics of rod-like macromolecules in concentrated solution. Part 1. J. Chem. Soc., Faraday Trans. 2, **74**, 560-570, 1978.
16. M. Doi, S.F. Edwards, The Theory of Polymer Dynamics, Clarendon Press, Oxford, 1987
17. F. Dupret, V. Verleye. Modelling the flow of fibre suspensions in narrow gaps. In D.A. Siginer, D. De Kee, R.P. Chabra (Ed.), Advances in the Flow and Rheology of Non-Newtonian Fluids, Rheology Series, Elsevier, 1347-1398, 1999.
18. J. Ferec, E. Abisset-Chavanne, G. Ausias, F. Chinesta. The use of interaction tensors to describe and predict rod interactions in rod suspensions. Rheologica Acta, **53/5-6**, 445-456, 2014.
19. F. Folgar, Ch. Tucker. Orientation behavior of fibres in concentrated suspensions. J. Reinf. Plast. Comp., **3**, 98-119, 1984.
20. G.B. Jeffery. The motion of ellipsoidal particles immersed in a viscous fluid. Proc. R. Soc. London, **A102**, 161-179, 1922.
21. M. Kroger, A. Ammar, F. Chinesta. Consistent closure schemes for statistical models of anisotropic fluids. Journal of Non-Newtonian Fluid Mech., **149**, 40-55, 2008.
22. R. Mezher, E. Abisset-Chavanne, J. Ferec, G. Ausias, F. Chinesta. Direct simulation of concentrated fibre suspensions subjected to bending effects. Modelling and Simulation in Materials Science and Engineering, **23**, 055007, 2015.
23. R. Mezher, M. Perez, A. Scheuer, E. Abisset-Chavanne, F. Chinesta, R. Keunings. Analysis of the Folgar & Tucker model for concentrated fibre suspensions via direct numerical simulation. Composites Part A, **91/1**, 388-397, 2016.
24. M. Perez, A. Scheuer, E. Abisset-Chavanne, F. Chinesta, R. Keunings. A multi-scale description of orientation in confined suspensions involving rods. Journal of Non-Newtonian Fluid Mechanics, **233**, 61-74, 2016.
25. M. Perez, S. Guevelou, E.Abisset-Chavanne, F.Chinesta, R. Keunings. From dilute to entangled fibre suspensions involved in the flow of reinforced polymers.Journal of Non-Newtonian Fluid Mechanics, **250**, 8-17, 2017.
26. J. Phelps, Ch. Tucker. An anisotropic rotary diffusion model for fibre orientation in short and long fibre thermoplastics. Journal of Non-Newtonian Fluid Mech., **156/3**, 165-176, 2009.

27. E. Pruliere, A. Ammar, N. El Kissi, F. Chinesta. Recirculating flows involving short fibre suspensions: Numerical difficulties and efficient advanced micro-macro solvers. Archives of Computational Methods in Engineering, State of the Art Reviews, **16**, 1-30, 2009.
28. S. Ranganathan, S.G. Advani. Fiber-fiber interactions in homogeneous flows of nondilute suspensions. J. Rheol., **35/ 8**, 1499-1522, 1991.
29. A. Scheuer, E. Abisset-Chavanne, F. Chinesta, R. Keunings. Second-gradient modelling of orientation development and rheology of confined suspensions. Journal of Non-Newtonian Fluid Mechanics, **237**, 54-64, 2016.
30. S. Toll. Note: On the tube model for fiber suspensions. J. Rheol., **37/l**, 123-125,1993.
31. S. Toll. Packing mechanics of fiber reinforcements. Polymer Engineering and Science, **38/8**, 1337-1350, 1998.
32. J. Wang, C.A. Silva, J.C. Viana, F.W.J. van Hattum, A.M. Cunha, Ch. Tucker. Prediction of fibre orientation in a rotating compressing and expanding mold. Polymer Engineering and Science, 1405-1413, 2008.
33. J. Wang, J. O'Gara, Ch. Tucker. An objective model for slow orientation kinetics in concentrated fibre suspensions: Theory and rheological evidence. Journal of Rheology, **52/5**, 1179-1200, 2008.
34. C. M. van Wyk. Note on the compressibility of the wool. Journal of the Textile Institute Transactions, **37:12**, T285-T292, 1946.